

# X-ray variability of AGNs in the soft and the hard X-ray bands

V. R. Chitnis

*Department of High Energy Physics, Tata Institute of Fundamental Research, Mumbai 400005, India*

J. K. Pendharkar

*Indian Institute of Astrophysics, II Block, Koramangala, Bangalore 560 034, India, and Physical Research Laboratory, Ahmedabad - 380 009*

D. Bose<sup>1</sup>

*Department of Astronomy and Astrophysics, Tata Institute of Fundamental Research, Mumbai 400005, India*

V. K. Agrawal

*Department of Astronomy and Astrophysics, Tata Institute of Fundamental Research, Mumbai 400005, India*

A. R. Rao

*Department of Astronomy and Astrophysics, Tata Institute of Fundamental Research, Mumbai 400005, India*

R. Misra

*Inter-University Center for Astronomy and Astrophysics, Post Bag 4, Ganeshkhind, Pune-411007, India*

## ABSTRACT

We investigate the X-ray variability characteristics of hard X-ray selected AGNs (based on Swift/BAT data) in the soft X-ray band using the RXTE/ASM data. The uncertainties involved in the individual dwell measurements of ASM are critically examined and a method is developed to combine a large number of dwells with appropriate error propagation to derive long duration flux measurements (greater than 10 days). We also provide a general prescription to estimate the errors in variability derived from rms values from unequally spaced data. Though the derived variability for individual sources are not of very high significance, we find that, in general, the soft X-ray variability is higher than those in hard X-rays and the variability strengths decrease with energy for the diverse classes of AGN. We also examine the strength of variability as a function of the break time scale in the power density spectrum (derived from the estimated mass and bolometric luminosity of the sources) and find that the data are consistent with the idea of higher variability at time scales longer than the break time scale.

*Subject headings:* black hole physics — galaxies: active — galaxies: nuclei — galaxies: Seyfert — X-rays: galaxies

## 1. Introduction

Time variable X-ray emission is a probe to the inner regions of the Active Galactic Nuclei (AGN) and is considered to be one of their defining characteristics. X-ray variability studies provide insight into the geometry and the physical conditions in the nuclear regions on account of the fact that this emission is thought to be emitted from regions close to the supermassive black hole. The X-ray variability studies on time-scales of months to years in AGNs have established the similarity of the physical processes across stellar mass to supermassive black holes (Uttley & McHardy 2004; McHardy et al. 2006). Since the characteristic time-scale is proportional to the mass of the black hole,  $M_{BH}$ , continuous monitoring for a long duration becomes necessary in the case of AGN based on linear scaling with black hole mass from X-ray binary systems.

Early studies on X-ray variability using data from *EXOSAT* in the 0.1 – 10 keV range showed that on short time-scales AGN variability appeared to be red noise dominated. In other words, it was unpredictable and aperiodic in nature (McHardy & Czerny 1987). Corresponding power spectral density (PSD, that is, variability power as a function of temporal frequency) is best fitted by a power-law of slopes -1 to -2 with no cut-off seen down to the lowest sampled frequencies. However, the shapes of their PSDs were shown to be similar to those of X-ray binaries (XRBs) in their soft state (McHardy 1988). Hence analogous to the high-frequency breaks seen in the PSDs of XRBs and assuming the break time-scale varying linearly with  $M_{BH}$ , a break to flatter PSD slope was expected over a period of days to weeks. Due to the uneven sampling of data the results yielding the break-frequency were uncertain. The *EXOSAT* data of a  $\sim$ day-long AGN X-ray observations have revealed inverse correlation between the amplitude of variability and X-ray luminosity (Barr & Mushotzky 1986). Results from the *ROSAT* All-Sky Survey (RASS) on the soft X-ray variability of AGN showed the variability strength on timescales of days to be a function of steepness of the X-ray spectrum with sources with steeper spectra exhibiting stronger

variability (Grupe et al. 2001). PSD studies were constrained due to large time gaps between subsequent observations in *ROSAT* data.

With the launch of the *RXTE* in 1995, a significant improvement was seen in the quality of data and a manifold increase in the monitoring timescale, from months to years, was possible. Because of its rapid slewing capability and flexible scheduling, an evenly sampled long-term monitoring of AGN X-ray variability was carried out for several sources. Contrary to the results from the then existing satellites, AGN light curves from *RXTE/PCA* in the 2 – 20 keV energy band showed that on longer timescales, of about a month, sources displayed less dispersion in variability amplitudes compared to those measured on time scales of 1 day (Markowitz & Edelson 2001). The PSDs also revealed a cutoff/ break at long timescales correlated with their black hole mass (Edelson & Nandra 1999; Uttley et al. 2002; Markowitz et al. 2003). but with a large scatter in the correlation (Done & Gierlinski 2005). McHardy et al. (2006) ascribed this scatter to a third variable, accretion rate, and found that the break time scale combined with accretion rate can predict the mass of the black hole all the way from Galactic X-ray binaries to supermassive AGNs. They postulated that the variability originates within the accretion disk and the break time scale is associated with the inner edge of the disk, which makes an inward movement with an increasing accretion rate for a given black hole mass.

Since such a scenario makes a definitive suggestion of the accretion disk geometry, a study of variability with energy should be able to pin down the radiation processes in the inner accretion disk quite reliably. Recently, the variability studies of AGN at energies above 15 keV are carried out by Beckmann et al. (2007). The data of the first 9 months of the *Swift/BAT* all-sky survey in the 14 - 195 keV range of the 44 brightest AGN revealed a tendency of unabsorbed or type 1 Seyfert galaxies to be less variable than absorbed or type 2 objects. Also they found a more solid anti-correlation between variability and luminosity, which was previously detected in soft X-rays, UV and optical bands.

The *RXTE/ASM* all-sky survey data gives information on a large number of X-ray sources,

---

<sup>1</sup>present address : Universidad Complutense, E-28040 Madrid, Spain

including AGNs. The sensitivity (typically 10 mCrab for the one day average data) is not sufficient to make a detailed study of AGNs. By taking data at larger bin sizes, however, it should be possible to get meaningful information on the variability at longer time scales. In this paper, we have carried out a comparative study of the variability of AGN in soft ( $< 12$  keV) and hard ( $> 12$  keV) X-ray bands using data from the *RXTE/ASM* all-sky survey and results obtained by Beckmann et al. from *Swift/BAT* all-sky survey. Data selection is described in section 2 followed by data analysis and results in section 3 and discussion and conclusions in section 4.

## 2. Data Selection

The All-Sky Monitor (ASM, Levine et al. (1996)) onboard Rossi X-ray Timing Explorer (*RXTE*, Swank (1999)) consists of three Shadow Scanning Cameras (SSCs). Each SSC contains a position-sensitive proportional counter (PSPC) that views sky through a slit mask. FOV of each SSC is  $6^\circ \times 90^\circ$ , allowing ASM to scan most of the sky every 1.5 hours. So apart from locating transient objects, it also provides photometric records of known sources in three energy bands corresponding to A (1.5 – 3 keV), B (3 – 5 keV) and C (5 – 12 keV) in addition to the total, or sum band, intensity in the 1.5 – 12 keV band. The MIT database ([http://xte.mit.edu/ASM\\_lc.html](http://xte.mit.edu/ASM_lc.html)), from where we have extracted ASM light curves, gives data dwell by dwell and one day average data points. In dwell by dwell each raw data point represents the fitted source flux from one 90 second dwell. Whereas in case of 'one day average' each data point represents the one-day average of the fitted source fluxes from a number (typically 5 – 10) of individual ASM dwells.

To have a comprehensive information, we have selected all AGN candidates (147) from the ASM source list and carried out a systematic analysis. We found 31 AGN from the sample used by Beckmann et al. (2007). We find measurable ASM flux for all the sources except two (NGC 1365 and GRS 1734-292). This sample of common sources consists of 3 blazars, 1 radio galaxy, 8 Seyfert 1, 4 Seyfert 1.5, 2 Seyfert 1.8, 1 Seyfert 1.9 and 12 Seyfert 2. The BAT sources not in the ASM source list include 1 blazar, 3 Seyfert 1, 1

Seyfert 1.5 and 8 Seyfert 2.

## 3. Data Analysis and Results

### 3.1. ASM dwell data selection criteria

We have downloaded all available ASM dwell data for 147 AGN from MIT database ([http://xte.mit.edu/ASM\\_lc.html](http://xte.mit.edu/ASM_lc.html)). This covers data from MJD 50087 to about 54466, i.e. 1996 January 5 to 2008 July 15. Dwell data are subjected to the usual selection cuts as prescribed by the ASM website and binned in 20 and 40 days bins. On closer inspection of light curves of individual sources, several large spikes, some of them with an apparent periodicity of one year, were noticed. These abnormal data were found to have large intrinsic errors too. Since the count rates in ASM is based on a profile fitting method, the errors depend on the other sources in the field of view and the orientation of the ASM FOV for a given observation. As a first cut, we examined the possibility that there could be enhanced unaccounted systematic errors for data points with large measured errors. It is found that the measured errors for each dwell data is sharply peaked at 1 counts/s. The distribution of errors for each dwell data for one of the sources (IC4329A) is shown in Fig. 1. Based on these considerations, we have introduced a selection criterion of an upper limit on sum count rate error of 3 counts/s, corresponding to thrice the peak value of the distribution.

After selecting dwell count rates for sum, A, B and C bands based on the above mentioned cuts, they are binned into 20 and 40 days starting from MJD 50087. For each bin the average rate and error are calculated for all the four bands, which are weighted mean and estimated error of the mean. Data points with too few number of individual dwell measurements (less than 20 data points for 20 day binning and less than 40 data points for 40 day binning) are also ignored, ensuring that there is at least one dwell per day, on an average. For example, for IC4329A, Fig. 2 shows the sum band rate error after binning as a function of number of dwells per bin, for 20 and 40 days binning. In both the cases sum band error increases sharply for bins with lower number of dwells. After introducing these criteria, the individual light curves are carefully examined and no systematic abnormalities are found in these light curves.

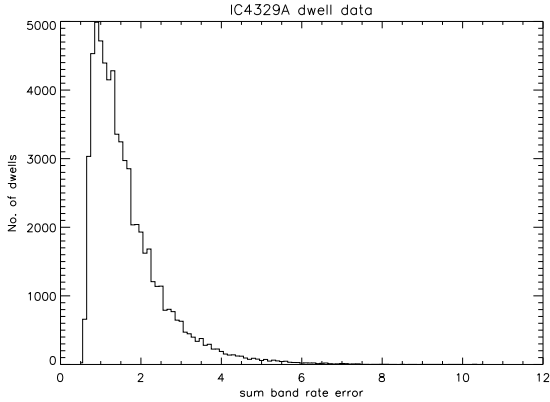


Fig. 1.— Distribution of errors on sum band rates from dwells for IC4329A

To summarize, the selection criteria for generating ASM light curves are:

1. Reduced chi-square of the fit  $< 1.5$
2. Number of sources in the field of view  $< 16$
3. Earth angle  $> 75^\circ$
4. Exposure time  $> 30$  seconds
5. Long-axis angle  $-41.5^\circ < \theta < 46^\circ$
6. Short-axis angle  $-5^\circ < \phi < 5^\circ$
7. Error on sum count rate  $< 3$  counts/s
8. Number of dwells for N day bin light curve is  $> N$

The first six selection criteria are the same as those used for generating one-day average count rates from dwell data as described in the MIT database webpage.

### 3.2. ASM light curves

The ASM measurements have a systematic error of 3% added in quadrature to the statistical errors. This error is estimated using Crab light curves and could be underestimate in some cases ([http://xte.mit.edu/ASM\\_lc.html](http://xte.mit.edu/ASM_lc.html)). Grimm et al. (2002) have studied light curves of several sources with constant X-ray flux binned with different bin durations from 1 to 200 days and have estimated systematic error on large time scales in the range of 0.01-0.1 cts/s, depending on the source flux. According to Fig. 2 of their paper, there seems to be a shift of about 10% between measured and estimated RMS for sources with constant flux. We have investigated this in detail to get a better handle on the average systematic errors. For a few of the bright sources, we have generated the power spectral density spectra (PSD) using a method based on the autocorrelation function (Gilfanov & Arefiev 2005) and have assumed that the frequency independent power has to be due to the errors in each observations. Based on these PSD, rms noise level seems to be underestimated by a factor of 1.13. A few steady sources too were investigated and the frequency independent systematic error is similar to this number. Though we cannot completely rule out some additional frequency dependent systematic

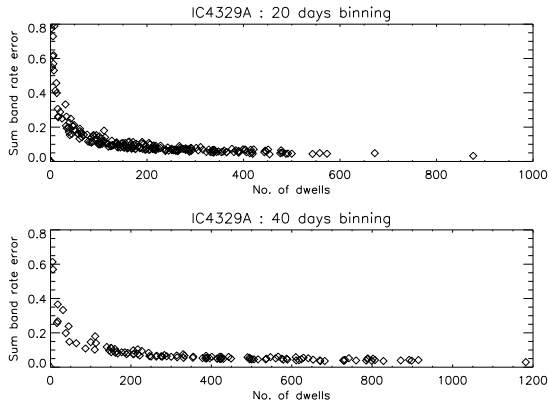


Fig. 2.— Sum rate error vs. no. of dwells for IC4329A with 20 days and 40 days binning.

errors, we assume that for large bin sizes (greater than 10 days), most of the systematic errors are taken into account. This assumption is further strengthened by examining individual light curves as well as the distribution of the source fluxes (see below). After correcting typical binned error of 0.005 c/s with this factor, this systematic error translates into typical systematic error of 0.5 c/s for dwell in S band and 0.3 c/s for A, B and C bands.

According to ASM data products page (<http://xte.mit.edu/>), there is a 1 mCrab positive bias in the light curve intensities. This bias is only evident when enough data are averaged so that the statistical uncertainties are driven to be very small. This generally requires binning or analyzing the light curves on time scales of many days or longer. In order to estimate this bias we have carried out the following exercise. We have generated histogram of average sum band count rates for 147 AGN (Fig. 3). Unlike the usual number distribution given in an integral way, this is a differential plot and hence the number should vary with count rates as a power-law with an index of -2.5 for an isotropic distribution. Hence we have fitted this histogram with a function consisting of a power-law with slope -2.5 and constant offset represented as the start point of the power-law. Count rates were spread in the X-axis using a Gaussian distribution with  $\sigma=0.0056$  counts/s according to the above mentioned error estimation. Fit for sum band data is shown in the Fig. 3. The number distribution is shown as data points with error bars (error taken is the square root of the number in each bin) and the fit is shown as a histogram. Offsets obtained with this method for various bands are as follows: S band : 0.0895 c/s, A band : 0.0274 c/s, B band : 0.015 c/s and C band : 0.0213 c/s. These values are consistent with the 1 mCrab offset quoted in the ASM website.

As a further verification of these offsets and systematic error, we checked for consistency of flux estimates. We compared our results with the flux obtained from an uniform spectral analysis done on a large sample of AGNs (Winter et al. 2009) and found 22 common sources. Using the spectral parameters from Winter et al. (2009) and ASM sum band average count rates we estimated 2–10 keV absorbed flux for these

sources using web calculator (WebPIMMS tool at <http://heasarc.gsfc.nasa.gov/Tools>). Fig. 4 shows the plot of ten years averaged absorbed ASM flux vs observed flux from other experiments, both in the energy range of 2–10 keV. It should be noted that these observations are not simultaneous. Hence source variability can cause non-identical fluxes between the ASM and the other experiments. Points are marked by diamonds. Solid line corresponds to the case where ASM flux is equal to flux measurements from other experiments. Dotted lines correspond to ASM flux equivalent to  $\pm 0.1$  c/s around solid line. Most of the sources barring a few like IC4329A and NGC 4388 are close to the fitted line, within  $\pm 0.1$  ASM c/s. As a further check we compared the long duration RXTE PCA measurements from the uniform analysis done by Markowitz & Edelson (2004). We found these measurements for nine sources: IC4329A, NGC4151, NGC3783, MCG-6-30-15, 3C120, 3C390.3, NGC3227, NGC4051 and NGC3516 (Markowitz & Edelson 2004). We estimated the ASM flux by extracting 40 days binned sum band rates near simultaneous with the PCA measurements. These points are indicated by plus signs with error bars in the plot. Hence overall there is a good agreement between flux estimates from ASM and other observations. This agreement also justifies our estimates of count rate offsets and systematic errors. We note here that further refinement in the flux comparison is difficult to achieve because of the fact that at shorter time scales (where pointed observations are available) ASM error bars are too large and at longer time scales (when the ASM error bars are driven to a small value) pointed observations are simply not available.

Applying the above mentioned cuts and corrections, light curves in all four bands were generated for all ASM detected AGNs. Average sum band count rates of all these AGN in four bands with 20 days binning for 30 sources common to ASM and BAT database are given in Table 1. There was one more common source, GRS 1734-292, which was rejected after applying above the mentioned cuts. That is, there was not a single stretch of 20 days with at least 20 dwells satisfying all the cuts (possibly because of its proximity to the Galactic center). Count rates given in Table 1 are weighted mean of binned counts rates and estimated error

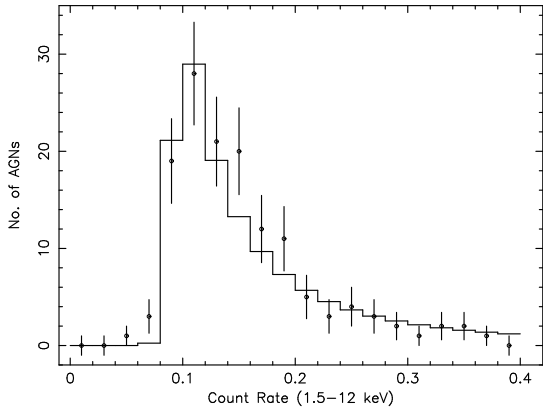


Fig. 3.— Histogram of ASM Sum band count rates for 147 AGN. Data is shown as points with error bars and the fit by power law with constant offset is shown as a histogram.

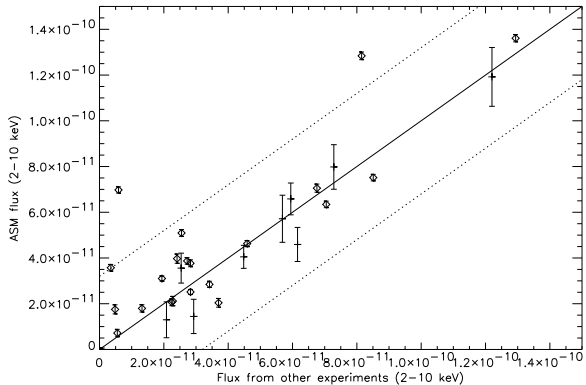


Fig. 4.— Absorbed ASM flux vs observed flux (in units of  $\text{ergs cm}^{-2} \text{s}^{-1}$ ) from various experiments shown by diamonds. ASM flux is derived from average of ASM count rate over the period of more than ten years. Solid line corresponds to the case where ASM flux is the same as flux from other measurements. Dotted lines correspond to ASM flux in the range of  $\pm 0.1$  count/s around solid line. Points indicated by plus signs (and large error bars) correspond to flux measurements from PCA onboard RXTE compared with simultaneous ASM measurements for IC4329A, NGC4151, NGC3783, MCG-6-30-15, 3C120, 3C390.3, NGC3227, NGC4051 and NGC3516.

on mean. Out of these, 15 sources have average sum band count rates above 0.2 counts/s. Some of these sources (11) are common sources in BAT and ASM database and are included in Table 1. The remaining sources are 1ES1959+650, IGR J18027-1455, MCG 6-30-15 and Mrk 501. Light curves for these 15 sources with 20 days binning are given in Figs. 5, 6 and 7.

The literature survey for RXTE-PCA light curves of AGNs (in this study) accumulated over long periods has allowed us to compare them with those of long looks of ASM. We could obtain PCA light curves for Mrk 501 and Mrk 421 taken over a period of 8 and 9 years respectively overlapping with the period for ASM light curves. The data set for Mrk 421 covers a period 1996-2005 (Figure 1 of Emmanoulopoulos & Wagner (2007)) and 1997-2004 for Mrk 501 (Gliozzi et al. 2006). Peaks at similar MJDs are identified on inspecting the ASM and PCA light curves for Mrk 421. The peaks were found near MJDs - 51000, 51700, 51900, 52600 and 53100. Similarly, peaks for Mrk 501 were found near the time 1997 (MJD 50600).

### 3.3. Variability strength

We have calculated the strength of variability for all these sources in bin sizes of 20 and 40 days. The strength of variability and the errors on them are calculated as follows.

Light curve from source consists of  $N$  flux measurements  $x_i$  with measurement errors of  $\sigma_i$ . In addition to these variations, object has intrinsic variability or additional source variance  $\sigma_Q$ . It is necessary to disentangle these two variances. One of the approaches to estimate the intrinsic variability is to use an *excess variance*  $\sigma_{XS}$  as an estimator (Nandra et al. 1997; Vaughan et al. 2003). It is given by

$$\sigma_{XS}^2 = S^2 - \overline{\sigma_i^2} \quad (1)$$

where the sample variance  $S^2$  is given by

$$S^2 = \frac{1}{N-1} \sum (x_i - \bar{x})^2 \quad (2)$$

where  $\bar{x}$  is mean rate and  $\overline{\sigma_i^2}$  is average variance of the measurements.

For light curves with varying measurement uncertainties ( $\sigma_i \neq \text{constant}$ ), it is necessary to use a numerical approach to obtain the best estimate for the parameter of interest ( $\sigma_Q$ , here)

TABLE 1  
VARIABILITY STRENGTH AND  $T_{Break}$  FOR ASM SAMPLE

Source name	ASM rate (1.2-15 keV) counts s <sup>-1</sup>	ASM luminosity log(L <sub>ASM</sub> ) ergs s <sup>-1</sup>	ASM variability strength <sup>1</sup> S <sub>v</sub>			BAT <sup>1</sup> variability strength S <sub>v</sub>	BH Mass (log M <sub>BH</sub> ) Msun	log(L <sub>bol</sub> ) ergs s <sup>-1</sup>	log(T <sub>B</sub> ) days	Type
			1.5-12 keV	1.5-3 keV	3-12 keV					
3C273	0.280±0.004	45.68	34.7±3.4	64.7±7.9	33.6±4.4	15±5	7.22	47.35	-3.04	Blazar
3C454.3	0.078±0.006	46.59	...	...	...	42±12	9.17	47.27	1.13	Blazar
Mrk421	0.894±0.005	44.57	83.7±4.2	79.4±4.1	88.4±4.5	142±38	8.29	~45.00	1.51	Blazar
IGR J21247+5058	0.126±0.004	43.54	42.3±5.0	...	51.4±5.0	11±6	...	...	...	Radio galaxy
3C120	0.173±0.005	44.11	42.7±6.3	64.1±7.9	38.9±10.4	≤10	7.42	45.34	-0.65	Sy1
3C390.3	0.109±0.004	44.37	29.7±5.3	49.6±9.4	30.5±7.5	≤6	8.55	44.88	2.17	Sy1
EXO0556-386	0.069±0.005	43.74	...	76.8±14.1	...	≤9	...	...	...	Sy1
IC4329A	0.459±0.006	43.91	22.7±2.5	48.0±4.5	18.1±3.5	≤3	6.77	44.78	-1.47	Sy1
MR2251-178	0.134±0.005	44.57	51.2±8.4	96.7±22.5	42.3±13.5	≤7	...	...	...	Sy1
NGC3783	0.222±0.005	43.16	28.5±4.9	67.3±12.8	24.1±7.4	≤4	6.94	44.41	-0.75	Sy1
NGC4593	0.105±0.005	42.76	79.7±11.2	...	71.3±21.8	≤7	6.91	44.09	-0.50	Sy1
NGC3227	0.125±0.005	42.10	56.2±7.1	123.2±17.6	49.3±11.4	≤14	7.64	43.86	1.26	Sy1.5
NGC3516	0.091±0.004	42.68	76.6±7.0	...	72.0±9.6	≤7	7.36	44.29	0.25	Sy1.5
NGC4051	0.064±0.005	41.31	...	...	...	≤9	6.13	43.56	-1.62	Sy1.5
NGC4151	0.434±0.005	42.51	53.9±3.2	136.3±12.5	53.3±3.2	27±7	7.13	43.73	0.32	Sy1.5
NGC1365	<0.005	...	...	...	...	≤17	...	...	...	Sy1.8
MCG-05-23-016	0.263±0.005	43.11	32.8±3.6	...	32.2±4.6	6±4	7.60	44.21	2.85	Sy1.9
NGC5506	0.237±0.006	42.79	42.9±4.6	...	47.7±5.2	≤3	8.00	44.53	1.36	Sy1.9
CenA	0.674±0.006	42.19	32.7±1.9	73.4±7.9	35.9±2.0	10±2	8.38	43.0	3.66	Sy2
CygnA	0.331±0.005	44.85	25.8±2.4	36.0±4.1	27.7±3.0	≤7	9.40	46.0	2.86	Sy2
ESO103-G35	0.120±0.006	43.16	69.5±9.0	76.8±14.1	74.3±10.1	≤8	...	...	...	Sy2
Mrk348	0.054±0.006	42.91	...	...	...	12±10	7.21	44.27	-0.04	Sy2
NGC1275	2.541±0.005	44.73	4.62±0.41	5.6±0.8	4.7±0.5	≤14	8.51	45.04	1.93	Sy2
NGC2110	0.168±0.005	42.84	41.7±5.3	69.7±13.9	28.4±7.6	25±7	8.30	44.10	2.41	Sy2
NGC2992	0.122±0.005	42.69	101.7±8.1	128.1±14.4	118.6±11.1	45±19	7.72	43.92	1.37	Sy2
NGC3081	0.022±0.005	41.98	...	...	...	23±11	...	...	...	Sy2
NGC4388	0.204±0.004	42.99	17.6±7.8	36.0±10.6	32.6±15.3	11±4	...	...	...	Sy2
NGC4507	0.062±0.006	42.77	...	...	...	≤8	...	...	...	Sy2
NGC7172	0.063±0.006	42.52	...	...	...	12±9	...	...	...	Sy2
NGC7582	0.056±0.005	42.02	...	...	...	23±21	...	...	...	Sy2
Mrk3	...	...	...	...	...	±7	8.65	44.54	2.72	Sy2
1ES1959+650	0.243±0.003	44.26	55.8±3.0	56.9±3.4	60.4±3.6	...	...	...	...	Blazar
IGRJ18027-1455	0.254±0.010	43.64	42.3±5.0	77.1±14.7	70.4±12.1	...	...	...	...	Sy1
MCG-6-30-15	0.208±0.006	44.65	34.3±5.7	69.1±7.8	40.2±8.7	...	6.65	43.56	-0.52	Sy1
Mrk 501	0.368±0.004	43.27	76.7±3.9	62.1±3.6	90.4±4.7	...	9.21	...	...	Blazar
Crab	75.355±0.010	...	0.48±0.03	1.25±0.07	0.37±0.03	1.27	...	...	...	Pulsar

<sup>1</sup>ASM variability strengths computed for data spanning duration of 12.5 years, whereas BAT variability strengths correspond to data collected over 9 months. Bin size is 20 days for both the cases.

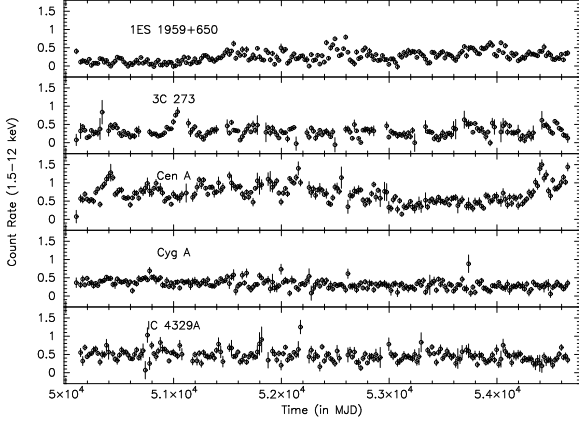


Fig. 5.— ASM Sum band light curves (1.5–20 keV) for 1ES 1959+650, 3C 273, Cen A, Cyg A and IC 4329A with 20 days binning.

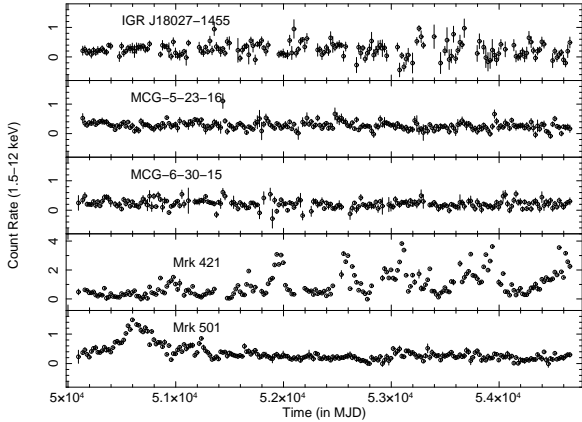


Fig. 6.— ASM Sum band light curves (1.5–20 keV) for IGR J18027-1455, MCG-5-23-16, MCG-6-30-15, Mrk 412 and Mrk 501 with 20 days binning.

(Almaini et al. 2000). The most widely used method for this purpose is the principle of maximum likelihood. The probability density of obtaining data values  $x_i$  is given as a product of Gaussian functions. Using Bayes' theorem probability distribution for  $\sigma_Q$  is obtained. This is likelihood function for  $\sigma_Q$  and it can be calculated assuming Bayesian prior distribution for  $\sigma_Q$  and  $x_i$ . By differentiating, maximum likelihood estimate can be obtained for  $\sigma_Q$  (see Beckmann et al. (2007) for equations). In the case of identical measurement errors ( $\sigma_i = \text{constant}$ ) this expression reduces to excess variance for uniform prior. This corresponds to  $\sigma_Q = \sigma_{XS}$ . In the present analysis of ASM data, since  $\sigma_i$  is almost constant, we have used this simplified approach. This assumption about approximate constancy of  $\sigma_i$ s is established using IC4329A data. Fig. 8 shows the distribution of sum rate error after 20 days and 40 days binning, after applying cut on no. of dwells per bin. Mean value of binned sum rate error and RMS is given in the figure. These distributions are sufficiently narrow to validate the assumption of constancy of  $\sigma_i$ s.

Variability is given in terms of normalized excess variance, i.e.  $\sigma_{NXS}^2 = \sigma_{XS}^2 / \bar{x}^2$  or the fractional root mean square (rms) variability amplitude ( $F_{var}$ ) given by

$$F_{var} = \sqrt{\frac{S^2 - \sigma_i^2}{\bar{x}^2}} \quad (3)$$

Error on variability or normalized excess variance consists of two parts: 1. arising from measurement error and 2. arising from intrinsic fluctuations, depending on the index of the power spectrum. So  $err(\sigma_{NXS}^2)$  is given by

$$[err(\sigma_{NXS}^2)]_T^2 = [err(\sigma_{NXS}^2)]_M^2 + [err(\sigma_{NXS}^2)]_I^2 \quad (4)$$

where subscript T stands for total error, M for measurement error and I for intrinsic error. According to equation (11) from Vaughan et al. (2003),

$$[err(\sigma_{NXS}^2)]_M^2 = \frac{2}{N} \frac{(\overline{\sigma_i^2})^2}{\bar{x}^4} + \frac{4\overline{\sigma_i^2} F_{var}^2}{N \bar{x}^2} \quad (5)$$

Also approximating intrinsic fluctuations with white noise (it should be noted that the light curves are red noise and white noise is assumed

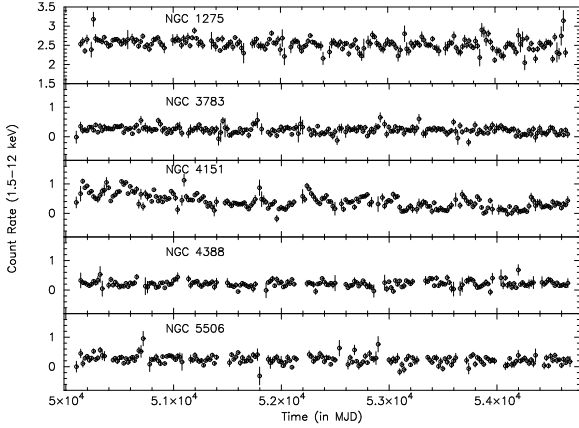


Fig. 7.— ASM Sum band light curves (1.5–20 keV) for NGC 1275, NGC 3783, NGC 4151, NGC 4388 and NGC 5506 with 20 days binning.

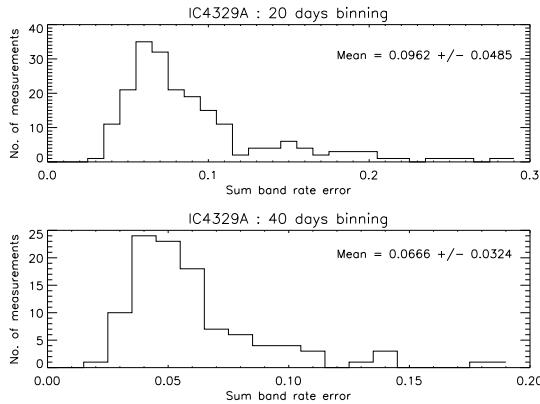


Fig. 8.— Distribution of sum rate errors with 20 days and 40 days binning for IC4329A after cut on number of dwells.

here for simplicity) and following Vaughan et al. (2003),

$$[err(\sigma_{NXS}^2)]_I = \sqrt{\frac{2}{N}}\sigma_{NXS} = \sqrt{\frac{2}{N}}F_{var} \quad (6)$$

Combining equations 5 and 6 we get

$$[err(\sigma_{NXS}^2)]_T^2 = \frac{2}{N} \left( \frac{\sigma_i^2}{\bar{x}^2} + F_{var}^2 \right)^2 \quad (7)$$

Substituting for  $F_{var}$  from equation 3 we get

$$[err(\sigma_{NXS}^2)]_T^2 = \frac{2}{N} \left( \frac{S^2}{\bar{x}^2} \right)^2 \quad (8)$$

Hence

$$[err(\sigma_{NXS}^2)]_T = \sqrt{\frac{2}{N}} \frac{S^2}{\bar{x}^2} \quad (9)$$

Following equation (B2) of Vaughan et al. (2003),

$$err(F_{var})_T = \frac{1}{2F_{var}} err(\sigma_{NXS}^2) \quad (10)$$

This is valid when  $err(\sigma_{NXS}^2)$  is small and we get the following expression

$$err(F_{var})_T = \frac{1}{\sqrt{2N}} \frac{S^2}{\bar{x}^2 F_{var}} \quad (11)$$

When  $err(\sigma_{NXS}^2)$  is large, the error estimate will only be approximate. The strength of variability is calculated from the expression  $S_V = 100\% \cdot \sigma_Q / \bar{x}$  i.e.  $S_V = 100\% \cdot F_{var}$ .

We have applied this method to downloaded light curves with different binning (20 and 40 days), and estimated  $\sigma_Q$  i.e. intrinsic variability as well as variability strength  $S_V$  for all ASM detected AGN. This exercise is carried out for sum band light curve over 1.5–12 keV, A band i.e. 1.5–3 keV, as well as (B+C) band i.e. 3–12 keV. Variability strengths for 20 and 40 days binning were found to be similar. Results for 20 days binning for sum band data are given in Table 1 for 30 AGN which are common between ASM and BAT database. We have also listed ASM variability strengths for four AGNs with ASM count rates above 0.2 c/s, but not detected by BAT. Also included in the table is BAT variability strength Mrk 3, which is not detected by ASM. In view of unknown systematics in ASM data, we have quoted ASM variability strengths in various bands

for only sources with count rates above 0.0895 c/s for S band and 0.0274 c/s for A band. BAT variability strengths given in this table are from Beckmann et al. (2007). We have quoted their results as upper limits for the sources where their estimates of variability strength are negative or smaller than error on estimate.

Since the X-ray spectral parameters (like the power-law index) are not available to all these sources, we have calculated the X-ray luminosities by converting the ASM sum band rates (R counts/s) to energy flux using

$$F[\text{erg}/\text{cm}^2/\text{s}] = 3.2 \times 10^{-10} \times R[\text{cts}/\text{s}] \quad (12)$$

This assumes Crab-like spectrum, as prescribed by Grimm et al. (2002). It should be noted that this assumption is not strictly valid for absorbed sources. For these sources photon index, over the A band in particular, could be much flatter than that of Crab. For the sources where spectral parameters are available, we get an average conversion factor very close to this value ( $3.0 \times 10^{-10} \times R$  [cts/s]).

To compare the flux in Crab units we have used a conversion factor of 75.5 counts/s (ASM sum band) and 453.8 counts/s for BAT rates as given by Beckmann et al. (2007). This allows easy comparison of fluxes in two different energy bands. Fig. 9 shows variation of BAT flux vs ASM total flux in the energy range of 1.5–12 keV. Blazars are indicated with plus signs, Seyfert 1 with asterisks, Seyfert 1.5 with diamonds, Seyfert 1.8 and 1.9 by square, Seyfert 2 with triangles and radio galaxy with a cross. Error bars are indicated for both BAT and ASM fluxes. Typically these error bars are smaller than symbol size. One Blazar, Mrk 421 and one Seyfert 2 galaxy, NGC1275 (not shown in the figure) seem to have much higher flux in ASM compared to other AGN with similar flux values in BAT energy band. Mrk 421 is highly variable source as can be seen from the ASM light curve. BAT data corresponds to only 9 months out of 12.5 years of data accumulated by ASM. (Mrk 421 was in a somewhat low state during the BAT observations.) In case of NGC 1275, ASM flux is about 33.7 mCrab whereas BAT flux is 4.5 mCrab. The field of view of NGC 1275 contains the Perseus cluster and X-ray emission from this cluster could be responsible for higher count rate and dilution of observed X-ray variability as

indicated by much lower variability strength for this source (Sanders & Fabian 2007). Solid line in the figure indicates both fluxes being linearly related (as will be the case if the spectral slope of AGNs is crab like - a photon index of 2). BAT flux seems to be increasing rapidly relative to the ASM flux. The lack of a strong correlation between ASM and BAT fluxes could be due to the mixing of different types of objects: sources with very soft spectrum which could be preferentially observed by the ROSAT satellite do not show flux correlation between the soft and hard bands (Tueller, Mushotzky, Barthelmy et al. 2008), whereas heavily obscured sources are obviously are not expected to show correlation (because the very soft flux in these sources may not be originating from the central engine of the AGN).

Fig. 10 shows luminosity of AGN from BAT data as given by Beckmann et al. (2007) vs ASM luminosity. On logarithmic scale BAT luminosity seems to be increasing with ASM luminosity linearly. There are two AGN which are slightly away from the trend shown by other AGN. These are Blazar : Mrk 421 and Seyfert 2 : NGC 1275 as in the case of Fig. 9.

Fig. 11 shows the plot of ASM and BAT variability strength in different energy ranges. Top panel shows ASM variability strength in 1.2–3 keV band, second panel shows ASM variability strength in 3–12 keV band and third panel shows BAT variability strength in 14–195 keV as a function of ASM variability strength in 1.5–12 keV range. Bottom panel also shows BAT variability strength in 14–195 keV as a function of ASM variability strength in 1.5–12 keV range, for near simultaneous data. Here we have selected ASM data corresponding to first nine months of BAT operation. Error bars on ASM variability strength in this panel are large and for some of the sources only upper limits on variability strength could be estimated for ASM data. For the sake of clarity we have restricted X-axis range to 120 for all the panels. Bottom-most panel has three points with ASM variability strength exceeding this value. Solid line in each panel corresponds to slope 1. It can be seen that variability strength decreases with increase in energy from 1.2–3 keV to 14–195 keV. Variability strength in 3–12 keV band seems to be well correlated and almost similar to the one in 1.5–12 keV band indicating that in these two

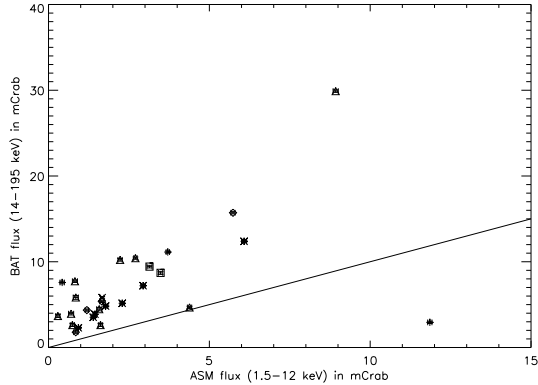


Fig. 9.— BAT flux (14-195 keV) vs. ASM flux (1.5-12 keV) for a sample of 30 AGN common in BAT and ASM data base. Blazars are indicated with +, Seyfert 1 by asterisk, Seyfert 1.5 by diamond, Seyfert 1.8 and 1.9 by square, Seyfert 2 by triangle and radio galaxy by cross. Solid line indicates slope 1.

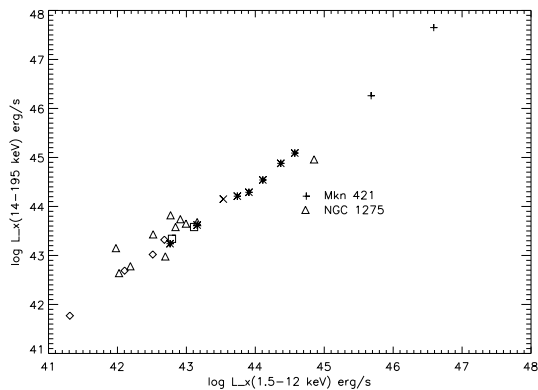


Fig. 10.— Hard X-ray luminosity of AGN from BAT vs soft X-ray luminosity from ASM for 30 common AGN. Blazars are indicated with +, Seyfert 1 by asterisk, Seyfert 1.5 by diamond, Seyfert 1.8 and 1.9 by square, Seyfert 2 by triangle and radio galaxy by cross.

energy bands most of the flux is in the large overlapping energy range. To investigate this further we have grouped the sources in three groups, 1. 3 Blazars and one radio galaxy, 2. 7 Seyfert 1 and 4 Seyfert 1.5 galaxies and 3. 1 Seyfert 1.8, 2 Seyfert 1.9 and 11 Seyfert 2 galaxies. Fig. 12 shows distributions of variability strengths in 1.5–12 keV, 1.5–3 keV, 3–12 keV and 14–195 keV bands. Dotted line corresponds histogram generated including all sources, dashed line corresponds to blazars i.e group 1 and solid line corresponds to Seyfert 1 and 1.5, i.e. group 2. This figure includes BAT variability strengths given as upper limits in Table 1. Average values of variability strengths for different groups and for different energy ranges are listed in Table 2. Values given here are the weighted mean and estimated error on the mean. BAT variability strengths given as upper limits in Table 1 are not included here. NGC 1275 is excluded here for ASM in these calculations since variability strength for this object quoted here could be grossly underestimated due to contamination caused by Perseus cluster in the field of view of ASM. This table clearly shows the trend of decrease in variability strength with increase in energy for all types of AGN.

Higher variability strength in 1.5–3 keV band compared to the one in 3–12 keV band for Seyfert 1’s is consistent with previous findings (see Arévalo et al. (2008) and references therein). They have found that the variability as a function of energy peaks around 2 keV one time scales of one to a few days. Our result extends this property to longer time scales.

We have compared our results with the variability strength in 2–12 keV from RXTE/PCA as presented by Markowitz & Edelson (2004). They have given variability strength for several Seyfert 1 and 1.5 galaxies on different time scales. There are five sources common between their sample with timescale of 1296 days (Table 3 in their paper) and the present sample. These are 3C120, NGC 3783, NGC 3516, MCG-6-30-15 and NGC 3227. For these sources we have computed average variability strength in the energy range of 1.5 – 12 keV with 40 days binning covering roughly the same MJD range as Markowitz & Edelson (2004). Bin size of 40 days used here is close to 34.4 days bin size used by them. Fig 13 shows the comparison of ASM variability strengths in 1.5 – 12 keV with

TABLE 2  
AVERAGE VARIABILITY STRENGTHS IN DIFFERENT ENERGY RANGES

Energy Range	All sources	Blazars	Sy 1-1.5	Sy 1.8-2
ASM (1.5-12 keV)	41.1±0.8	57.3±1.7	38.4±1.4	34.1±1.2
ASM (1.5-3 keV)	61.4±1.5	64.7±2.0	64.0±2.9	51.5±3.0
ASM (3-12 keV)	44.3±1.0	64.2±1.9	39.1±1.9	36.4±1.4
BAT (14-195 keV)	12.6±1.3	17.2±3.6	19.2±5.3	11.4±1.5

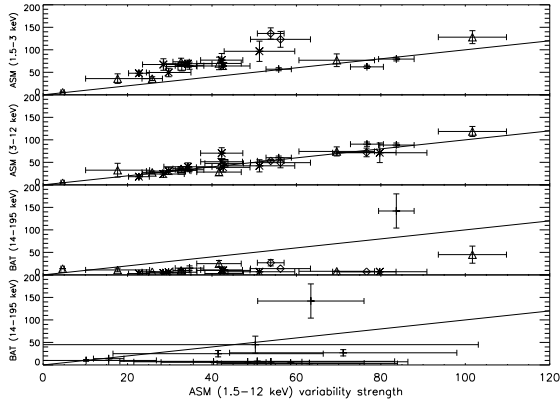


Fig. 11.— (a) ASM variability strength in 1.5-3 keV band, (b) ASM variability strength in 3-12 keV band (c) BAT variability strength in 14-195 keV band as a function of ASM variability strength in 1.5-12 keV band and (d) BAT variability strength in 14-195 keV band as a function of ASM variability in 1.5-12 keV band for simultaneous data. Variability strength decreases at higher energies.

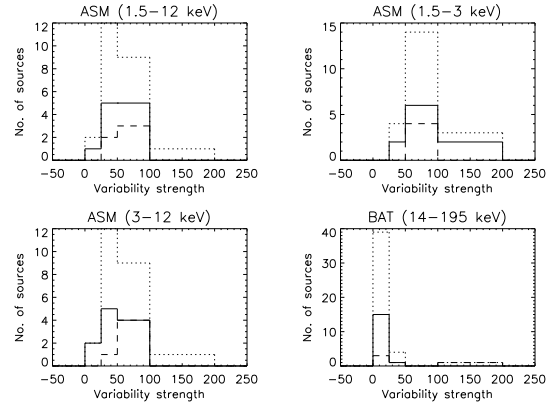


Fig. 12.— Distribution of variability strengths of AGN in (a) 1.5–12 keV, (b) 1.5–3 keV, (c) 3–12 keV and (d) 14–195 keV as obtained from ASM and BAT data. In each panel, dotted line represents distribution including all objects, dashed line corresponds to blazars and radio galaxy and solid line represents variability strength distribution for Seyfert 1 and 1.5.

PCA variability in 2 – 12 keV range. ASM variability seems to be higher than the PCA variability.

### 3.4. Variability strength vs break time scale

AGN variability is often expressed in terms of fluctuations in power spectral density (PSD) i.e. variability power  $P(\nu)$  as a function of frequency,  $\nu$ . On longer timescales, the PSDs of AGN are fitted by a power-law of slope -1 which breaks to a steeper slope ( $> 2$ ) at timescales shorter than the 'break' timescale,  $T_B$  (Markowitz et al. 2003). Break timescale is expected to depend on the black hole mass. Considering similarities between PSDs of X-ray binaries and AGN, break timescales for AGN are expected to be in the range of  $\lesssim 1$  day to  $\gtrsim$  a hundred days. Earlier attempts of comparing the  $T_B$  with black hole mass ( $M_{BH}$ ) for AGN have shown a rough linear scaling but with a scatter (Markowitz et al. 2003; McHardy et al. 2004). Improving on it, an inverse dependence on a second variable, probably the accretion rate, was suggested (McHardy et al. 2004, 2005; Uttley & McHardy 2005). McHardy et al. (2006) quantified the relationship between  $T_B$ ,  $M_{BH}$  and  $L_{bol}$  (in place of the accretion rate), as  $\log T_B = A \log M_{BH} - B \log L_{bol} + C$ , where  $M_{BH}$  is in units of  $10^6$  solar masses,  $L_{bol}$  is bolometric luminosity in  $10^{44}$  erg  $s^{-1}$ . Best fit values determined by them are  $A (= 2.1)$ ,  $B (= 0.98)$  and  $C (= 2.32)$ . Using this relation, we have calculated break timescales ( $T_B$ ) for our AGN sample. Values of  $\log(M_{BH})$  (in units of  $10^6 M_\odot$ ) and  $\log(L_{bol})$  (in units of  $10^{44}$  erg  $s^{-1}$ ) listed in Table 1 are adopted from Woo & Urry (2002), Uttley & McHardy (2005) and Wandel & Mushotzky (1986). The masses are estimated either using reverberation mapping or the BLR size-luminosity relation or the stellar velocity dispersion method.  $L_{bol}$  values are also taken from references mentioned above. It should be noted that  $L_{bol}$  for the blazars may be beamed, leading to a wrong estimates of  $T_B$ .

Figure 14 shows ASM variability on the scale of 20 days as a function of  $\log(T_B)$ . Figure 15 shows BAT variability strength as a function of  $\log(T_B)$ . Out of 44 AGN from BAT sample of Beckmann et al. (2007), black hole masses and bolometric luminosity are available for 20 sources (Uttley & McHardy 2005), and hence  $T_B$  could

be estimated for these sources. Out of these, 19 sources are common between ASM and BAT database. The remaining source is Mrk 3, which is not in the ASM source list. Figure shows some increase in variability of BAT data for AGN in the neighborhood of 20 days and decrease on both lower and higher sides. The average variability for  $\log(T_B)$  between -1 to +1.6 is 62.9 and 53.6, for the ASM and BAT respectively and these values are 27.4 and 16.7 outside this range. The decrease for higher  $T_B$  is as expected. The lower variability at lower  $T_B$  could be due to a variety of reasons like a) inclusion of a blazar for which the McHardy et al (2006) relation may not be valid b) at very low value of  $T_B$ , we are sampling the sources at very low frequencies where a second turn-over of PSD is likely if the sources are a state like the low-hard states of Galactic black hole sources.

### 3.5. Energy spectra

We checked for data from pointed observations of these AGN by X-Ray Telescope (XRT) onboard Swift during this 9 month period. Data was available for four sources from our list. These were three Blazars : 3C273, 3C454.3 and Mrk 421 and one Seyfert 2 Galaxy : Cen A. We have fitted spectrum over the energy range of 0.3–10 keV for these four objects. For each of these objects source and background photons were selected using XSELECT version 2.4. For Photon Counting (PC) mode source photons were selected in a circular region with the radius of 20 pixels (i.e. 47 arc-seconds), whereas background photons were extracted from nearby circular region with a radius of 40 pixels. For data collected in Windowed Timing (WT) mode, source photons were extracted using box region with the length of 40 pixels and width about 20 pixels. Events with grades 0-12 and 0-2 were selected for PC and WT mode data, respectively. The spectral data were rebinned by GRPPHA 3.0.0 with 20 photons per bin. Standard auxiliary response files and response matrices were used.

Spectra for these sources were fitted using XSPEC version 12.3.1 with a model consisting of absorbed power law over the energy range of 0.3–10 keV. In each case  $N_H$  was fixed to the value given in Table 2 of Beckmann et al. (2007). Power law indices and 2–10 keV flux obtained from fit are given in Table 3. It should be noted here,

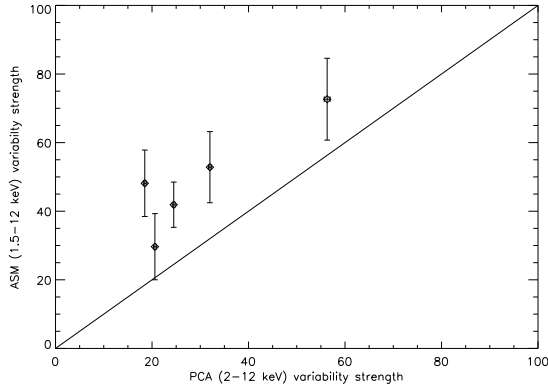


Fig. 13.— ASM variability strength (1.5–12 keV) vs RXTE PCA variability strength (2–12 keV) for Seyfert 1 and Seyfert 1.5 galaxies.

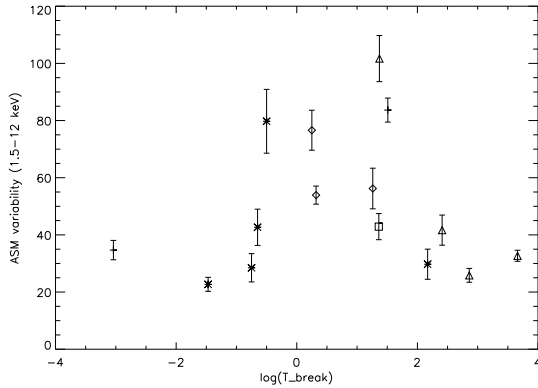


Fig. 14.— ASM variability strength vs break time scale  $T_{break}$ .

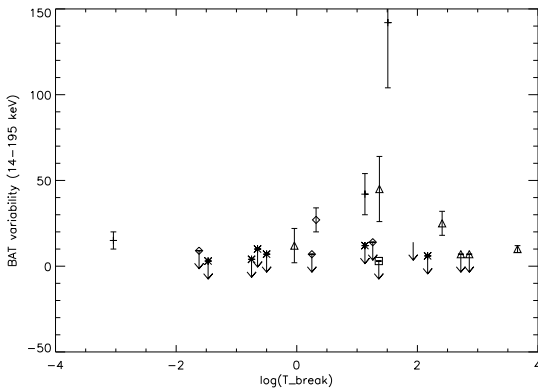


Fig. 15.— BAT variability strength vs break time scale  $T_{break}$ .

however, that the Swift observations may not be equal to the average photon index representing the ASM observations.

Among the three Blazars, Mrk 421 has the steepest spectrum and 3C 454.3 has the flattest one. In case of 3C454.3, we have not estimated the variability strength in ASM band because of low count rate. ASM variability strengths for other two blazars are :  $83.7 \pm 4.2$  for Mrk 421 and  $34.7 \pm 3.4$  for 3C273. Whereas BAT variability strengths of these three sources arranged in the order of increasing power-law index are : 3C454.4 ( $42 \pm 12$ ), 3C273 ( $15 \pm 5$ ) and Mrk 421 ( $142 \pm 38$ ). This indicates an increase in variability strength for sources with steeper spectra. But this inference should be taken with caution. It should be noted that in case of Mrk 421, which is a BL Lac type of object, the hard X-ray band is dominated by high energy synchrotron emission whereas in case of 3C454.3 and 3C273, which are FSRQ, hard X-ray emission is mainly inverse-Compton emission. This could be the one possible reason for steeper spectrum of Mrk 421 compared to the other two objects. It is also quite possible that the long duration variabilities of blazars are influenced by infrequent strong flare events and the higher variability in any one blazar could simply be the effect of a few large events which happen to occur in that source.

#### 4. Discussion and conclusions

Study of X-ray variability of AGN at longer time scales and also at different energies is very important to pin down the accretion disk geometry and the radiation processes involved in the X-ray emission very close to the black holes. We have made a systematic study of the soft X-ray variability characteristics of all AGN with measured long time scale variability from Swift/BAT.

One of the important findings of this work is that individual ASM dwells can be co-added to obtain flux integrated over long time scales and by propagating the measurement errors, very low errors on the data points are obtained. This method assumes that most of the systematic errors in the flux measurements in the individual dwell measurements are understood and taken care of. Support for this assumption comes from the fact that the long duration light curves of several AGN bear

TABLE 3  
SPECTRAL FITS

Source name	Observation duration s	$N_H$ $10^{22}\text{cm}^{-2}$	Powerlaw index	2-10 keV flux $\text{erg}/\text{cm}^2/\text{s}$
3C 273	2962.6	0.0316	$1.79\pm 0.030$	$5.87\times 10^{-11}$
3C 454.3	13670.0	0.0631	$1.32\pm 0.02$	$5.43\times 10^{-11}$
Mrk 421	6958.0	0.001	$2.38\pm 0.01$	$8.34\times 10^{-11}$
Cen A	7699.5	12.59	$1.64\pm 0.06$	$1.99\times 10^{-10}$

a striking similarity to the light curves obtained from pointed RXTE/PCA observations. Some more work, however, need to be done to understand possible time dependent systematic errors so that a complete data set can be used to derive meaningful power spectral densities.

Another important finding is the quite uniform variation of variability strength with energy for diverse classes of objects, except for the blazar Mrk 421. For this particular source, there is a marked increase in the variability as a function of energy. Such behavior has been observed at shorter durations. Horan et al. (2009) made a detailed multi-wavelength study for a period of about 300 days and find the variability to increase across the full electro-magnetic band. In particular, they noticed a sharp increase of variability from soft X-rays to hard X-rays: the values for variability ( $F_{var}$ ) were 26.9, 44.3, 52.9 and 99.3, respectively for Swift XRT, RXTE-ASM, RXTE-PCA and Swift-BAT data (for observation bins of a few tens of thousand seconds and duration in the range of 24 to 256 days). The values that we obtained are 79 (RXTE-ASM 1.5 – 3 keV), 88 (RXTE-ASM 3 – 12 keV) for 11 years and 142 (Swift-BAT for 300 days). The energy dependent variability behavior of the the blazar in our list, 3C 273, for which data is available both in the soft and hard X-rays, shows an energy dependent behavior similar to Seyfert 1 galaxies. McHardy (2006) has noted that the wide band PSD of 3C273 is identical to that of Seyfert galaxies and contended that the process responsible for variability in this source is the same that produces variability in non-beamed sources.

Most of the other sources in our sample are Seyfert galaxies and a decrease in the variability

as a function of energy is observed. In a detailed study of a large number of Seyfert galaxies based on the first seven years of RXTE-PCA monitoring, Markowitz & Edelson (2004) give energy dependent variability data for long durations and a similar trend of decrease in variability with energy has been noticed. There are five Seyfert 1 galaxies (3C120, 3C390.3, IC4329A, NGC3783, and MCG-6-30-15) and two Seyfert 1.5 galaxies (NGC4151 and NGC3227) common between their sample and our work. The ratio of variability for the soft (2 – 4 keV) and the hard (7 – 12 keV) band are, respectively, 1.15, 1.26, 1.19, 1.28, 1.37, 1.26 and 1.35, for a duration of 216 days. For comparison similar ratios from our data (1.5 – 3 keV vs 3 – 12 keV), for the above sources, respectively, are, 1.65, 1.62, 2.65, 2.9, 1.71, 2.6, and 2.5, for the full ASM duration. The typical uncertainties are 0.06 for the RXTE data and 0.3 for our data. Though this ratio from RXTE data is fairly same for all the sources (about 1.27), for the ASM data it varies from 1.66 to 2.64. For five sources energy dependent variability at longer times scales (> 16 days) is given by Markowitz et al. (2003) and for two of the sources where we have obtained very high ratio (NGC 3783 and NGC 4151) a sharp upturn towards lower energies are noticed (see their Fig 6). Further, RXTE-ASM is more sensitive to low energy X-rays. The effective area at 2 keV is about 33% of the effective area at 5 keV (Levine et al. 1996), whereas this number is < 1% for RXTE PCA (Jahoda et al. 2006), mainly due to the propane layer on the top side of RXTE-PCA which has lower transparency at low energies due to aluminized mylar windows and the permeation of xenon gas into the propane layer (Jahoda et al.

1996). Hence it is quite possible that the higher variability at low energies derived by us is real and indicate a sharp increase of variability in AGNs at lower energies for longer time scales. Though we cannot completely rule out some further systematic errors, it is quite evident that RXTE-ASM is an unique instrument to probe long time scale variability at lower energies.

There are, indeed, several indicators from early EXOSAT data which supports the above assertion. Walter & Courvoisier (1992) discuss X-ray variability of several AGNs observed by EXOSAT over the period of an year and note that soft X-rays vary by factors up to 7, much higher than that seen in hard X-rays. Two of the sources in their list is common to the present work: MR2251-178 and NGC 3783. For these two sources, they report a peak-to-peak variation of 4.5 and 3, respectively in the soft X-rays, compared to 1.9 and 1.8 in hard X-rays. This should be compared with the  $S_V$  derived by us for these two sources: 97 and 67, respectively in the 1.5 – 3 keV band and  $42 \pm 14$  and  $24 \pm 7$  in the 3 – 12 keV band, respectively. Though there is a strong indication of very high soft X-ray variability at long time scales, a detailed comparison with a large number of pointed observations for individual sources are required to pin down any residual systematic errors in the RXTE-ASM data.

Energy dependent variability has been studied extensively in Galactic black hole sources (see Zdziarski (2005) and references therein) and one of the models used to explain the energy dependency is the variations in the input parameters of the thermal Comptonization process which results in an pivoting power-law spectrum. Though the very low value of variability in the BAT energy band may be influenced by a non-varying spectral component in this energy band (like reflection), detailed wide band spectroscopy of Seyfert galaxies suggest a common continuous phenomena for the decreasing variability with increasing energy. For example, the radio galaxy 3C120 shows only a moderate reflection component and very strong spectral variability (over two days) with the spectral index correlated with the soft X-ray flux, indicating a phenomena where the input seed photon variation for a thermal Comptonization process causes the energy dependent X-ray variability (Zdziarski & Grandi 2001). If the same

phenomena is responsible for most of the sources reported in this work, it suggests that a) for a majority of AGNs the thermal Comptonization is the dominant process, b) the pivot energy is higher (greater than about 20 keV).

This work is based on results provided by the ASM/RXTE teams at MIT and at the RXTE SOF and GOF at NASA's GSFC. This research has also made use of data obtained from the High Energy Astrophysics Science Archive Research Center (HEASARC), provided by NASA's Goddard Space Flight Center. We are very grateful to the referee of this paper for the very thoughtful and critical comments.

## REFERENCES

- Almaini, O., Lawrence, A., Shanks, T., et al. 2000, MNRAS, 315, 325
- Arévalo, P., McHardy, I. M., Markowitz, A., Papadakis, I. E., Turner, T. J., Miller, L. & Reeves, J. 2008, MNRAS, 387, 279
- Barr, P. & Mushotzky, R. F., 1986, Nature, 320, 421
- Beckmann, V., Barthelmy, S. D., Courvoisier, T. J.-L. et al. 2007, A&A, 475, 827
- Done, C. & Gierlinski M., 2005, MNRAS, 364, 208
- Edelson, R. & Nandra, K. 1999, ApJ, 514, 96
- Emmanoulopoulos, D. & Wagner, S. J., 2007, The Central Engine of Active Galactic Nuclei ASP Conference Series, 373, 163
- Gilfanov, M. & Arefiev, V. 2005, arXiv:astro-ph/0501215
- Gliozzi, M., Sambruna, R. M., Jung, I., Krawczynski, H., Horan, D. & Tavecchio, F. 2006, ApJ, 646, 61
- Grimm, H.-J., Gilfanov, M. & Sunyaev, R. 2005, A&A, 391, 923
- Grupe, D., Thomas, H. C., & Beuermann, K. 2001, A&A, 367, 470
- Horan, D., Acciari, V. A., Bradbury, S. M. et al. 2009, astro-ph/0901.1225

- Jahoda, K., Swank, J. H., Giles, A. B. et al. 1996, Proc. SPIE, 2808, 59
- Jahoda, K., Markwardt, C. B., Radeva, Y. et al. 2006, ApJS, 163, 401
- Levine, A. M., Bradt, H., Cui, W. et al. 1996, ApJ, 469, L33
- Markowitz, A. & Edelson, R. 2001, ApJ, 547, 684
- Markowitz, A., Edelson, R., Vaughan, S. et al. 2003, ApJ, 593, 96
- Markowitz, A. & Edelson, R. 2004, ApJ, 617, 939
- McHardy, I. M. & Czerny, B. 1987, Nature, 325, 696
- McHardy, I. M. 1988, Mem. Soc. Astron. Ital., 59, 239
- McHardy, I. M., Papadakis, I. E., Uttley, P., Page, M. J. & Mason, K. O. 2004, MNRAS, 348, 783
- McHardy, I. M., Gunn, K. F., Uttley, P. & Goad, M. R. 2005, MNRAS, 359, 1469
- McHardy, I. M. 2006, Astronomical Society of the Pacific, 350, 94
- McHardy, I. M., Koerding, E., Knigge, C., Uttley, P. & Fender, R. P. 2006, Nature, 444, 730
- McHardy, I. M., Arévalo, P., Uttley, P. et al. 2007, MNRAS, 382, 985
- Nandra, K., George, I. M., Mushotzky, R. F., Turner, T. J., Yaqoob, T., 1997, ApJ, 476, 70
- Sanders, J. S. & Fabian, A. C. 2007, MNRAS, 381, 1381
- Swank, J. 1999, Nucl. Phys. B ( Proc. Suppl.), 69, 12
- Uttley, P., McHardy, I. M. & Papadakis, I. E. 2004, MNRAS, 332, 231
- Uttley, P. & McHardy, I. M. 2004, Progress of Theoretical Physics Supplement, 155, 170
- Uttley, P. & McHardy, I. M. 2005, MNRAS, 363, 586
- Vaughan, S., Edelson, R., Warwick, R. S., & Uttley, P. 2003, MNRAS, 345, 1271
- Walter, R. & Courvoisier, T. J.-L. 1992, A&A, 266, 57
- Wandel, A. & Mushotzky, R. F. 1986, ApJ, 306, L61
- Winter, L. M., Mushotzky, R. F., Reynolds, C. S. & Tueller, J. 2009, ApJ, 690, 1322
- Woo, J.-H. & Urry, C. M. 2002, ApJ, 579, 530
- Zdziarski, A. A. & Grandi, P. 2001, ApJ, 551, 186
- Zdziarski, A. A. 2005, MNRAS, 360, 816.

---

This 2-column preprint was prepared with the AAS L<sup>A</sup>T<sub>E</sub>X macros v5.2.